

## Article

# Development of a Transient Model of a Lightweight, Portable and Flexible Air-Based PV-T Module for UAV Shelter Hangars

Pedro Orgeira-Crespo <sup>1,\*</sup>, Carlos Ulloa <sup>1</sup> , José M. Núñez <sup>2</sup>  and José A. Pérez <sup>3</sup>

<sup>1</sup> Aerospace Area, Department of Mechanical Engineering, Heat Engines and Machines, and Fluids, Aerospace Engineering School, University of Vigo, 32004 Ourense, Spain; carlos.ulloa@uvigo.es

<sup>2</sup> Centro Universitario de la Defensa (Marín), University of Vigo, 36920 Marín, Spain; jnunez@uvigo.es

<sup>3</sup> Design Engineering Department, Industrial Engineering School, University of Vigo, 36310 Vigo, Spain; japerez@uvigo.es

\* Correspondence: porgeira@uvigo.es

Received: 11 May 2020; Accepted: 28 May 2020; Published: 5 June 2020



**Abstract:** This research paper introduces a mathematical model to predict the performance of photovoltaic–thermal systems (PV-T), based on a thin layer flexible panel and an air pipe, by using the Trnsys<sup>®</sup> software tool to simulate energetic systems. The main advantage of these types of panels is their easy portability, making them ideal to address thermal needs in several scenarios. In the military field, there is an important concern about the use of sustainable energy; for instance, cooling facilities for infantry tents used in their deployments. In this research, a PV-T panel to cover electrical power needs for an infantry’s hangar unmanned air vehicle (UAV) is introduced. The proposed thermal model, based on the novelty of inertial mass (lump) as an approach to real panel behavior, has been validated through the comparison between Trnsys’ model simulation data, a real weather station, and data obtained in a test bed. Genopt’s simulation software is used to fit the model, allowing for the prediction of heat transmission coefficient values. The good match between simulated and experimental data makes the proposed model suitable for the photovoltaic–thermal prediction of panel behavior.

**Keywords:** PV-T; Trnsys; optimization; lump; UAV

## 1. Introduction

Nowadays, photovoltaic and thermal panels are both used separately in new construction buildings, and solar electrical power is a consolidated source of energy. Their combined use is not new, where photovoltaic panels act as thermal absorbents into a photovoltaic–thermal system (PV-T). Recent advances in the PV-T field have resulted in the analysis of different technologies (as flat plane, or those based on solar concentrators), or in the study of the efficiency of several configurations [1,2]. Other research investigated new configurations, with special emphasis on plane and parabolic PV-T collectors [3–7]. Studies on PV-T focused on working fluids are also important, especially those that make the segmentation on air or water types: according to the nature of the working fluid, both system configurations and applications are different. Water cooling PV-T systems are more suitable for thermal energy storage but their complexity and fluid leaks risk prove to be a major disadvantage. Air cooling systems are simpler but have their own drawbacks as well: less efficient heat transfer and a more difficult thermal storage [3,8]; in addition, their combination might be risky, as shown in [9].

An interesting approach for flat plate is found in [10], where TRNSYS is used to model that type of solar photovoltaic systems, as in this research. It is very relevant since it summarizes the applications of PV-T, including their advantages and limitations. Research such as [11–16] is also significant in

that the different energy exchange models are analyzed, especially those air-type systems relevant for this paper. The most recent research in this field are focused on developing domestic applications for this type of systems [17], comparative studies of flat plate PV-T for different configurations [18,19], development, new technologies and applications of PV-T systems [20,21], and the analysis of PV-T arrangements from the point of view of exergy [22]. Experimental data is crucial to validate theoretical models for these systems, as in [23], with an especial focus on PV-T system's performance [24–28]. The results of the research carried out in [26,29,30] are specially related to the discussion of our analysis, since they validate experimental data with the simulation of the models they introduce. In Section 4, RMSE (root mean square error) and regression coefficient obtained for the actual output temperature in the experiments within our research, are compared to those obtained in the abovementioned references.

PV-T devices are energy multigeneration systems, since they generate two types of energy at the same time: both electric and thermal. There share certain similarities with cogeneration systems, where thermal engines are used to generate electricity, restoring residual heat. As more research has focused on multigeneration, different validation models have been proposed in the literature [31–33].

Most models have been developed under stationary state conditions, as in Stirling's engine-based micro-cogeneration system [34], but transient responses are needed for any HVAC (heating ventilation air conditioning) system simulation, since they very frequently turned on and off throughout a year. Although annual system efficiency of a Stirling Engine (SE) facility can be estimated using permanent state models, dynamical models are more suitable for these types of simulations, despite the fact that they present certain drawbacks depending on the type of system under study.

A complex system model definition generally requires a comprehensive analysis of design parameters, that sometimes are unknown (such as heat exchange surfaces, heat transfer coefficient, and material characteristics), which implies that such models have limited results. According to this, a valid approach is the use of a lumped mass, in order to model a Stirling engine-based micro-cogeneration system: two lumped (inertial) masses allow decoupling transient thermal model from system's geometry [35].

Throughout the scientific literature, different operative SE parameters have been extensively studied using concentrated mass transient models, and their influence on engine behavior has been researched [36–38]. These grouped parameter models constitute a valid method to successfully simulate different thermal machine behavior [39].

This research paper introduces a flexible, portable, lightweight and modular PV-T system to generate heat and electricity to the Spanish Navy Infantry's unmanned air vehicle (UAV) shelter hangars. These types of tents, designed for military environments, are especially dedicated to small aircraft hangars, vehicle installation facilities, and are a clear example of PV-T application for this purpose [40]. The proposed PV-T system is designed to be used by an eleven-infantry chalk that needs to deploy a small UAV hangar to store their short-range portable unmanned aerial vehicles, serve as a launch and return point for their aircrafts, as well as perform tactical and maintenance tasks. The PV-T system is required to provide heat (and keep inside temperature within standard values) and generated electrical power to charge drone batteries. Considering an eleven-module PV-T (one per soldier), each unit should provide at least 33.63 Wh/day; this premise was used to define the output power generated by the photovoltaic panel in the PV-T module. This is based on previous research, where geometry was designed based on the Analytical Hierarchical Process (AHP), using Ansys Fluent simulations to compare different design alternatives [41]. This paper introduces a thermal model based on a lumped mass; the thermal model is simulated using Trnsys, and optimized via GenOpt; in order to validate the model, an experimental setup is designed, and data are captured the whole year through.

In this research, a worst-case scenario is chosen to optimize the model, where a whole winter day has to be simulated with PV-T system transient, using concentrated lumped inertial mass. Transient model is implemented on TRNSYS software and is optimized using GenOpt. Simulation results are compared to experimental ones obtained in PV-T system test bed.

The rest of the paper is organized as follows: in Section 2.1, the experimental setup prepared to validate the theoretical model is introduced; Section 2.2 depicts the thermal model used, and the equations that mathematically represent it; Section 2.3 introduces simulation tools used to obtain the parameter values to be validated with experimental results; finally, Sections 3 and 4 discuss the result and show our conclusions.

## 2. Materials and Methods

### 2.1. Experimental Setup

To accomplish the validation of the theoretical model for the PV-T based on a flexible thin layer with experimental data, a workbench was implemented on the roof of one of the facilities in the Spanish Naval Military Academy. It was designed using SolidWorks, and manufactured for this project, as seen in Figure 1:

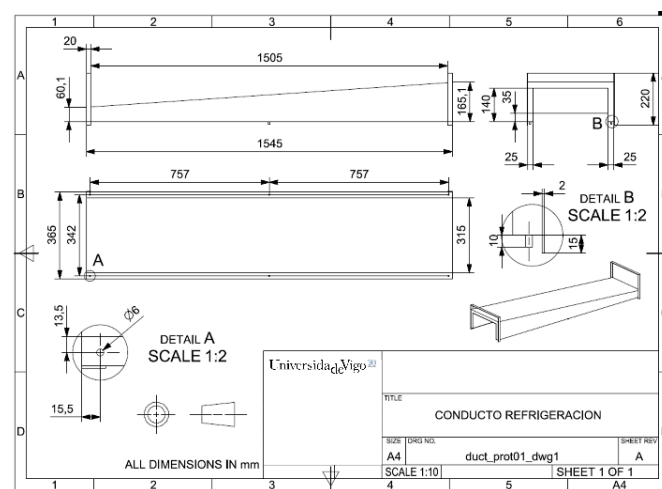


Figure 1. Detailed manufacturing blueprints for experimental setup.

It is made of a rollable Powerfilm R21 panel (fiberglass substrate), with a textile envelope wrapping a metallic structure, as developed for previous research [33]. A 150-mm long insulated cooling duct was connected on one side to extract heat; it is shown in Figure 2, and its diameter is 60 mm. Fluid inside the PV-T increases temperature because of panel heat that cannot be extracted through the other surfaces (that are adiabatic).



Figure 2. Detail on the cooling duct.

Air is extracted with the aid of two 140 mm diameter NF-A14 fans (Figure 3) that can provide a maximum flow of 182.5 m<sup>3</sup>/h per unit; they operate under PWM, so that flowrate can be controlled, up to a maximum of 8.2 g/s and 4.3 Watts. Figure 3 shows the fans integrated in the test bed:



**Figure 3.** Detail on the fans once installed.

The experimental setup was manufactured and then tested in the laboratory. Figure 4 shows the test bed with the PV-T panel:

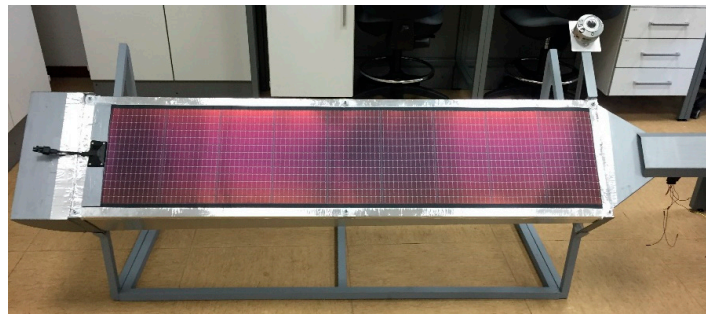


**Figure 4.** Manufactured experimental setup

And Figure 5 shows the data monitor station that was getting recorded information:



**Figure 5.** Manufactured experimental setup.

A specific mounting base was designed with a slope angle equal to test location's latitude ( $42.4^\circ$  N), with clamping plates for the different probes, as seen on Figure 3. PV's backsheet cooling duct is completely isolated from the environment and includes safety screens in both input and output that provide protection against Sun radiation effect on the sensors. The test bed includes a data acquisition system, specifically designed as a flexible, reliable and scalable solution to record and transmit remotely the data captured through its sensors. The core of the acquisition system is an Arduino board, chosen since it is a low-cost open source well known to authors, already used on similar cases [42–45]. Figure 6 shows test bed deployed in the top of a building in the Spanish Naval Military Academy:





Figure 6. (a) test bench; (b) test bench, fan view.

Figure 7 shows measuring point locations in the PV-T panel. For the thermal model, input ( $T_{in}$ ) and output ( $T_{out}$ ) refrigeration air temperatures, and airflow speed (FR) are logged. Environmental conditions are also logged, inasmuch as they are also relevant; wind speed is obtained using a meteorological station, and the incident radiation on PV-T panel (SI) is measured on workbench.



Figure 7. Test bench with different measuring probes highlighted.

This setup has been collecting data since January 2019, having an insight on a whole year of information (8760 h). On that dataset, a process aimed at purging outliers was carried out; moreover, we focused on the coldest days (worst case scenario), specifically eight days without erroneous or incomplete data. Recorded data are input and output air temperature, that can be found in Figure 8, where average hourly data obtained from two digital thermometer IC are displayed over that period of time (the raw data is captured every ten seconds and it is averaged every hour to be displayed in the figure):

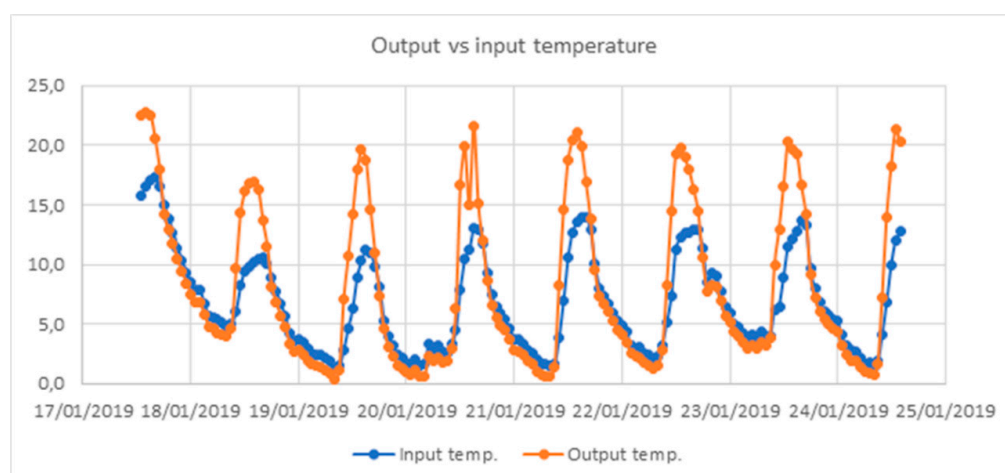


Figure 8. Measurements of collector outlet versus inlet temperature during one week.

Table 1 shows the parameters obtained on the workbench, the sensors used for every measurement, the measurement range, the type of output data, and the required power voltage. Instruments and actuators were integrated on the Arduino system by using different input mechanisms, as shown in the table. To analyze the different airflow conditions in the panel, the speed of the fans that push the air in the cooling duct are controlled by two industrial fans having flow regulation capability: Noctua NF-A14, regulated by a digital PWM signal that the Arduino system provides, for each fan. Since the dynamic of the plant is relatively “slow”, logging frequency is not critical, having thus reduced the sensing period to every 10 s.

**Table 1.** Instruments used in test bench.

Parameter	Number of Sensors	Sensor	Range	I/O Type	Power Supply
Temperature	2	DS18B20 Thermometer	−55–125 °C	Digital (One-Wire)	5 VDC
Flow rate	1	Bosch HFM 5 Air-mass meter	8–370 kg/h	Analog (0–5 V)	8–17 VDC
Solar irradiation	1	Kipp & Zonen SMP10 Pyranometer	0–1600 W/m <sup>2</sup>	Analog (4–20 mA)	5–30 VDC

## 2.2. Thermal Model

For the purpose of the validation of this heating system based on flexible PV-T on campaign facilities, a thermal model is designed, as shown in Figure 9. As may be seen, the air used to warm the small facility is the one from thermal system output.

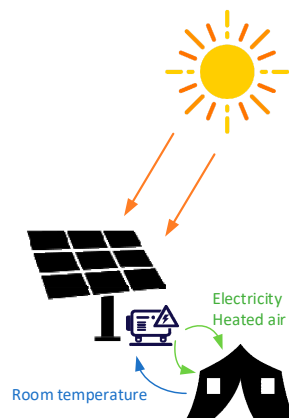


**Figure 9.** PV-T operating scheme: the system is provided with (cold) tent air and solar radiation, supplying heated air and electricity.

To estimate system output temperature, a heat exchange model is proposed. The panel surface is being heated by Sun’s radiation, that is logged through our instrumentation system described in the previous section. Obviously, output variables will depend on system location and incident radiation angle. Moreover, panel losses (physically due to radiation and convection) are computed and classified in internal losses (the one from panel surface to the cooling duct, due to convection), and external losses (due to radiation and convection); internal losses are responsible for air heating.

The proposed thermal model for the system will be represented as a lumped mass in Trnsys, as shown in Figure 4. This solution simplifies the heat transfer issue without accuracy loss. The main ideas behind lumped mass are: first, to assume that panel temperature is unique, constant through the whole panel; second, transfer coefficients are also constant and temperature independent. Consequently,

we assume that photovoltaic panel temperature is constant through the panel surface and will vary according to its thermal capacity (calculated as the product of multiplying the mass per its specific heat).

PV-T panel absorbs solar radiation and sets up a heat transfer with the environment at the same time. The system reaches a temperature that allows a convection towards passing fluid (air) passing through the system, provided that the temperature gradient allows heat transfer: energy losses suffered by lumped mass to the system will equal passing fluid absorbed energy, having only to perform an energetic balance to reach the desired output temperature.

Equation (1) depicts heat transfer rate, that will be equaled to convection losses as shown in this section. This is the total heating power received by the air that passes through PV-T pipe:

$$\dot{Q}[\text{J/s}] = \dot{m}c_p\Delta T \quad (1)$$

In this equation,  $\dot{m}$  is air's mass flow in cooling duct expressed in  $[\text{kg/s}]$ ,  $c_p$  is specific heat of air expressed in  $[\text{J/kg}\cdot\text{K}]$ , and  $\Delta T$  is the gradient temperature between input and output expressed in  $[\text{K}]$ .

Thermal energy undergoes different changes in its process from being radiated heat to becoming a means to condition the temperature of the facilities. First, irradiation “ $G$ ” is defined as the quantity of incident radiation per unit of surface and time. The ratio of total irradiation absorbed by panel surface is obtained by Equation (2):

$$\alpha G \quad (2)$$

where  $\alpha$  is solar absorptivity, and  $G$  is incident irradiation.

As shown in Figure 10, the part of the losses named “Losses 1” is divided in two parts: radiation losses and convection losses. As for exchanged heat, it can be defined according to Equation (3):

$$\dot{q}_{rad}[\text{W/m}^2] = \varepsilon\sigma(T_s^4 - T_{sky}^4) \quad (3)$$

where  $\varepsilon$  is panel emissivity,  $\sigma$  Stefan-Boltzmann's constant ( $5.67\cdot 10^{-8} \text{ W/m}^2\cdot\text{K}^4$ ),  $T_s$  the temperature in K of the surface in touch with the fluid, and  $T_{sky}$  surrounding surface temperature in K. The latter is estimated through environment temperature  $T_{amb}$  according to Swinbank's proposed model [46]:

$$T_{sky} = 0.0552 T_{amb}^{1.5} \quad (4)$$

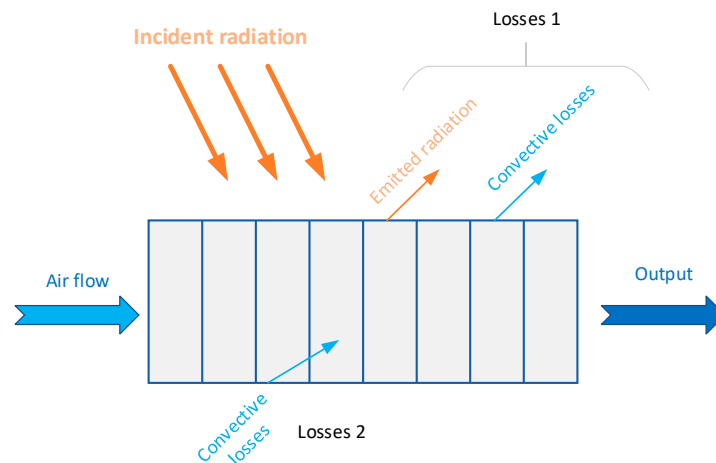


Figure 10. PV-T thermal model.

Not only panel surface temperature but also internal and external temperatures are computed by using the same parameter,  $T_s$ , since we are modeling PV-T panel as lumped mass. Moreover, convection losses to the outside can be defined using Equation (5):

$$\dot{q}_{conv} [\text{W/m}^2] = h(T_s - T_{amb}) \quad (5)$$

where  $h$  is convection heat transfer coefficient expressed in  $\frac{\text{W}}{\text{m}^2 \cdot \text{K}}$ , that will be estimated using recorded wind speed (in m/s), according to the classic model by Nusselt-Jürges [47]:

$$h = 5.8 + 3.95 V_w \quad (6)$$

As a result, heat flow perpendicular to panel surface can be written according to Equation (7).

$$-k \frac{dT_s}{dx} = h(T_s - T_{amb}) + \varepsilon \sigma (T_s^4 - T_{sky}^4) - \alpha G \quad (7)$$

Once losses to the outside have been defined, heat transfer from panel surface to the inside has to be identified. Being again a convection loss, it will follow the same Equation (5), only instead of using  $T_{amb}$ , the temperature to be used is the one the fluid is achieving along the cooling duct of the system. To perform this task an integration through the whole length of the pipe is necessary, since the air is going to increase temperature on its way. That gain results in a convectional power loss as the fluid progresses, the higher the temperature gradient, the faster the heat exchange; the gain is getting smaller, anyway, since inertial system temperature is the same regardless of its location, while that of air is increasing.

Consequently, to simplify calculations, an average temperature for the fluid in the pipe will be used. That assumption is valid since this heating system does not experiment great temperature gradients, and it will be calculated in the following section in a series of iterations (it is dependent on fluid's temperature at system's output, that is in fact unknown, and the value we are seeking).

Moreover, in this section the idea of using an energetic balance to obtain  $T_{out}$  was introduced. Up to this point, we already know that convectional energy losses through the panel corresponds to the energy that air flow is obtaining, so by using Equations (1) and (5) we may calculate the balance:

$$h_{in} A_{PV} (T_l - T_{ma}) = \dot{m} c_p (T_{out} - T_{amb}) \quad (8)$$

where  $A_{PV}$  is panel area,  $T_l$  lump mass temperature, and  $T_{ma}$  is the average temperature of the fluid inside. The temperature at the surface of the lump mass  $T_s$  is the temperature of the lump mass  $T_l$ , as per its definition, as shown in Equation (9).

$$T_s = T_l \quad (9)$$

The reason for defining in the same manner received radiation and panel's losses to the outside is that both directly affect the temperature that the lump mass achieves, so output temperature depends on both, as will demonstrated in this section.

As for the simulation, it will follow the layout shown in Figure 11, where the equations and parameters for lump mass temperature  $T_l$  are depicted and the relationship between that temperature and output's temperature get into a circular argument.  $T_{out}$ , thus, will be obtained as result of a series of iterations, and will be the temperature of the facility we are conditioning.

Obviously, this heating system is only useful as long as the output temperature (of facilities intake temperature) is higher than the temperature inside the facility. According to this, a sensor must be installed to compare both temperatures, activating a controller that stops air flow when heating system is really cooling it, instead of providing heat.



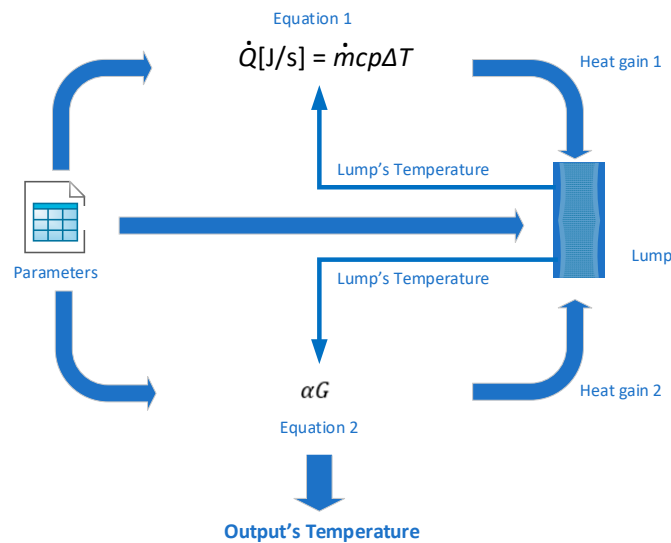


**Figure 11.** Block heat transfer scheme for the design of the thermal simulation.

### 2.3. TRNSYS Simulation

Lumped systems are those where body temperature varies over time, but in which that body temperature is also constant throughout its whole volume. The PV-T panel is not a true lumped system but, due to its slenderness, it can be modelled as such. Once this hypothesis has been formulated, PV-T thermal capacitance is then defined as the product of multiplying its mass by its specific heat.

The proposed model was implemented on TRNSYS, using the lump mass (Type963) as the core simulation concept. The great unknown when it comes to implement lump is the definition of its capacitance. That capacitance will be obtained by minimizing the gap (or error) between simulated data and the dataset obtained after selecting an average week. To solve this, a series of iterations are performed taking the capacitance as a changing variable and simulating iteratively until the minimum possible error is achieved. To do so, GenOpt software is used in conjunction with TRNSYS.

Previously shown heat transfer equations for the model are inserted as TRNSYS Equations in that software. For each module, energetic balances are computed. By applying collected climatological data to the model, the PV-T system output temperature is obtained.

TRNSYS implemented model can be seen in Figure 12.

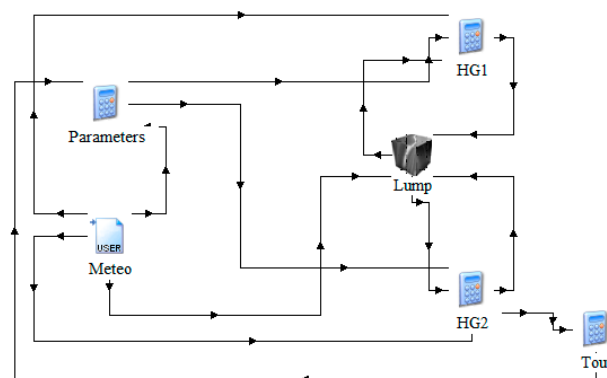


**Figure 12.** Thermal model TRNSYS implementation.

Heat gain 1 (HG1) computes energetical balance in the external surface, according to Equation (7). Heat gain 2 (HG2) performs energetical balance calculations according to the first term of Equation (8). The signs of both equations have to be changed, since for the lump mass energetical balance is not to be considered as a loss, but a gain.

The main parameters used to perform simulation are solar absorptivity and panel emissivity, both fixed to 0.7. Experimental values applied to the model are obtained for an air volumetric flow of 8.2 gr/s, pumped by the three fans the workbench has at the entrance of the pipe. Selected meteorological data are for the second week of January in Marin, at the Spanish Naval Military Academy.

### 3. Results

In the first place, experimental- and TRNSYS-simulated data are compared to find the minimum error between those values, according to the previous section. To perform the optimization, we try to find the mean square error (RMSE), according to Equation (10):

$$\text{RMSE} = \sqrt{\frac{1}{n} \sum_{i=1}^n (y_i - x_i)^2} \quad (10)$$

The value obtained for the lump mass' capacitance after minimizing RMSE up to 1.1 °C is 9.0134KJ/K, with a 0.98 regression coefficient. This RMSE value is obtained for an average experimental temperature of 7.8 °C and is within the validated values systems with similar characteristics throughout the literature. For instance, in [29], a validation of the experimental data obtained from a PV-T is performed, achieving a 1.11 °C value, for an actual temperature of 30 °C. Other similar RMSE results are also obtained in other scenarios where lumped mass is also applied. In reference [36], a Stirling engine block is modeled as a lump mass; the output temperature of the refrigeration water achieves a RMSE value of 1.0 °C, for a 45 °C block temperature. In that research, other different experimental scenarios for 60 and 70 °C block temperatures are also tested, resulting in RMSE values of the same order of magnitude (1.4 and 4.0 °C, respectively). In reference [26], an analysis of the regression coefficient is performed, achieving 0.95 and 0.98 values for output temperature, in the order of magnitude of those in our research.

The regression coefficient value obtained is within expectations and aligned with similar experimental validation tests. For example, in reference [30] a validation of experimental results for a PV-T panel is performed. In that research, the PV-T used water as refrigeration fluid and the value of the regression coefficient between actual output temperature and the simulated one is 0.99, very similar to our case (0.98).

Figure 13 shows actual temperature (red color), while simulated data are represented in the blue color. As can be appreciated in the figure, there are eight peaks corresponding to the eight simulated days, and maximum achieved radiation. The simulated data matches actual data reasonably well to expectations.

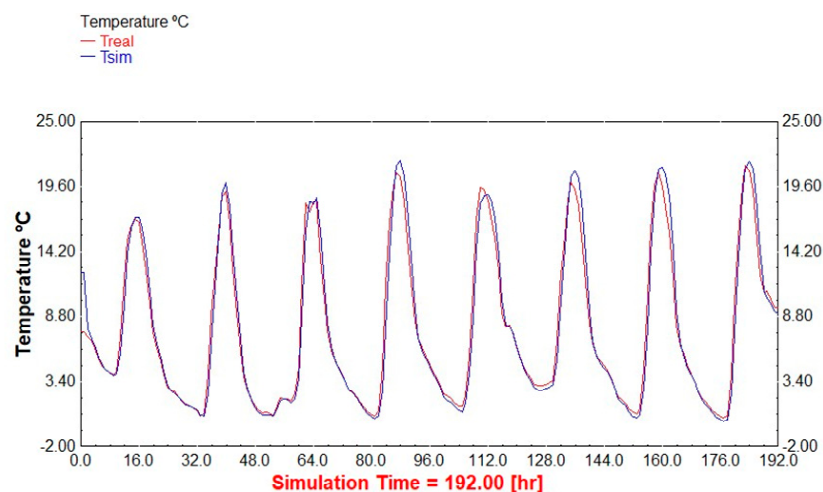


Figure 13. Experimental actual temperature ( $T_{\text{real}}$ ) versus simulated ( $T_{\text{sim}}$ ) during simulation period.

Figure 14 represents intake temperature versus output temperature obtained through simulation. According to the size of the gap between input and output, the system will have further thermal conditioning capabilities.

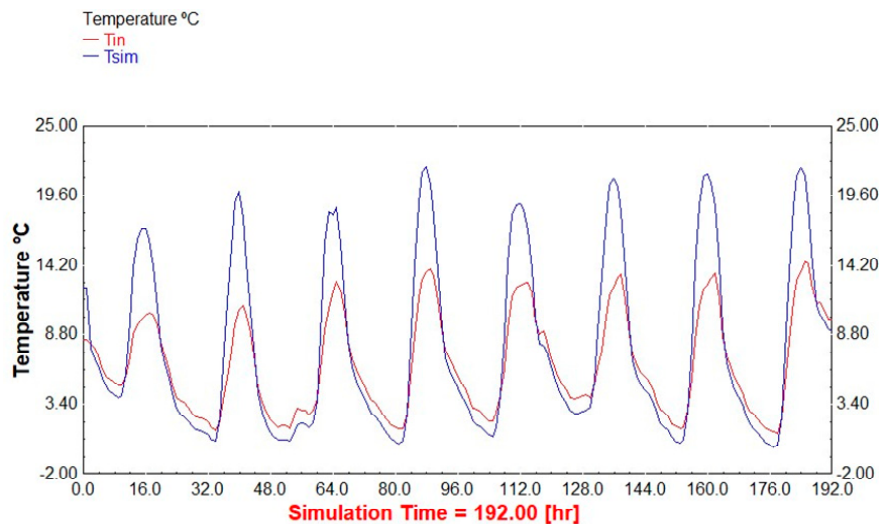


Figure 14. Output's simulated temperature ( $T_{sim}$ ) versus intake temperature ( $T_{in}$ ) in  $^{\circ}\text{C}$ .

The proposed system is validated, given its capability of increasing the temperature of the facilities to be conditioned. Table 2 shows the simulated output temperature peaks according to time, input temperature, and achieved gradient temperature. A maximum temperature increase of  $9.2\text{ }^{\circ}\text{C}$  is reached. This value allows for a generic room air conditioning up to a  $19.9\text{ }^{\circ}\text{C}$  limit, since that is the temperature of the air at the outlet of the duct. It is important to note that this system was originally designed to fulfil the demand of UAV shelter hangars; those are operational facilities (not for leisure) and, consequently, a small temperature increase immediately generates a thermal comfort sensation.

Table 2. Temperature increases during peak hours.

Simulation Step (h)	$T_{out}(^{\circ}\text{C})$	$T_{in}(^{\circ}\text{C})$	$\Delta T(^{\circ}\text{C})$
16	17.1	10.3	6.7
34	19.9	10.8	9.2
62	18.4	10.8	7.6
87	21.9	13.7	8.1
111	18.9	12.7	6.3
135	20.9	12.4	8.4
159	21.2	12.7	8.5
183	21.7	13.7	7.0

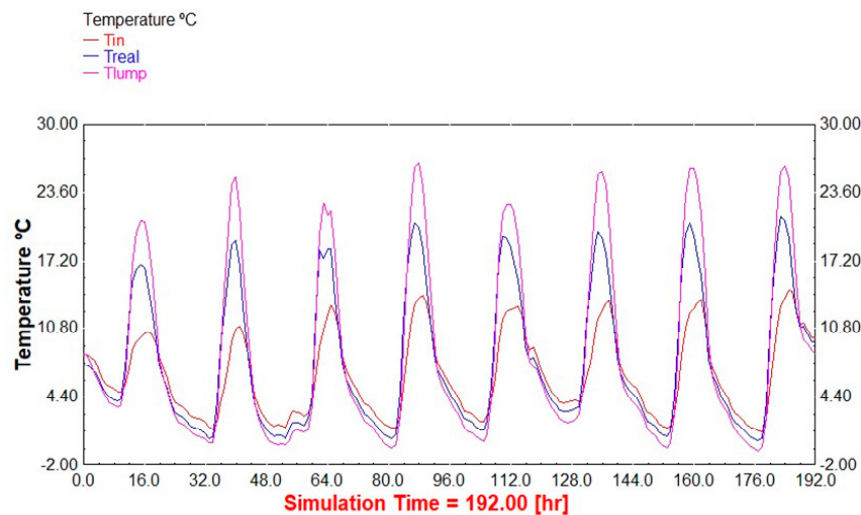
Another interesting analysis is the one focused on nightly periods where output temperature is below the one at the input. Considering the whole period of simulation time, we obtain an average temperature increase of  $1.2\text{ }^{\circ}\text{C}$ . If we limit analysis period to the phases where  $T_{out} > T_{in}$ , it happens for 72 out of the 192 h in total, which represents 37.5% of the whole time. Under these conditions, the average temperature increase reached is  $4.8\text{ }^{\circ}\text{C}$ , as Table 3 displays.

Table 3. Heating net time.

Period	$\bar{T}_{out}(^{\circ}\text{C})$	$\bar{T}_{in}(^{\circ}\text{C})$	$\Delta \bar{T}(^{\circ}\text{C})$
Simulation time (100%)	7.7	6.6	1.2
Heating time (37.5%)	14.9	10.0	4.8

It is reasonable to have a system working in a 37.5% cycle for heating purposes for a full year simulation, since nightly period takes most of the daytime during winter (when there are few hours of solar radiation).

As represented in Figure 15, during the night phase of the day, the temperature inversion phenomenon occurs: the input temperature is the one higher, followed by the output temperature, and finally, the lump mass temperature is the lowest. This is due to radiation heat exchange with the environment together with quite low sky temperatures during winter nights.



**Figure 15.** Actual output temperature ( $T_{\text{real}}$ ) versus input temperature ( $T_{\text{in}}$ ) versus simulated lump mass temperature ( $^{\circ}\text{C}$ ).

Finally, thermal gains HG1 and HG2 are shown. Figure 16 plots heat transfer rates 1 and 2 versus total incoming radiation. The scales are adapted to undoubtedly show that PV-T's performance as thermal collector is relatively small.

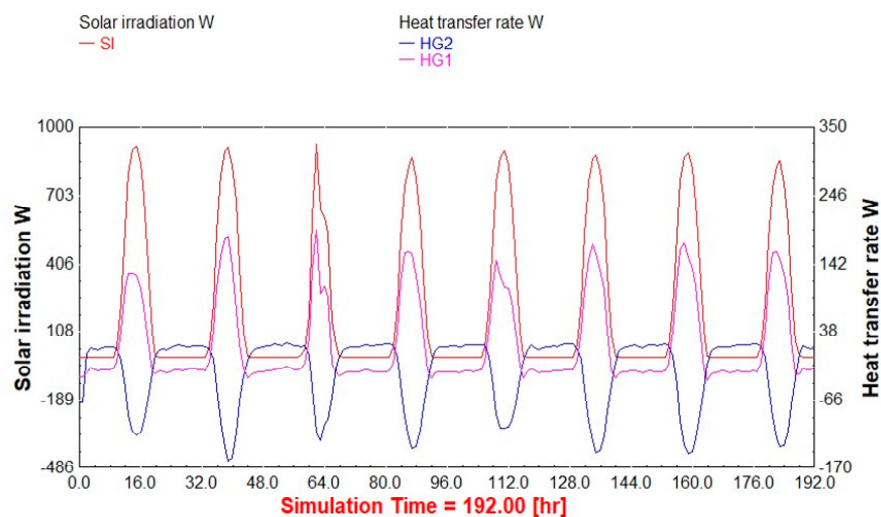


**Figure 16.** Incident radiation (SI) compared to thermal gains (HG1 and HG2).

As Figure 16 displays, HG2 is under zero values for most of the simulation time; the HG2, heat transfer rate for the lump mass, actually represents a heat loss towards the air inside the duct. This happens during daylight, but the opposite occurs at night; during the night, it is the lump mass that is

heated from the duct, since the air is still flowing inside the test bed, and ambient temperature is higher than that of the lump mass at that moment. As for the negative values of HG1, the reason is the heat loss that the lump mass suffers, interchanging that heat with the sky at night by means of radiation.

#### 4. Conclusions

According to the obtained results, we conclude that the proposed model is validated through experimental results. PV-T's thermal modelling as lump mass is not only possible, but also a great concordance between the workbench's data and simulated values. Root mean square error achieved, 1.1 °C, and regression coefficient (0.98) are considered reasonable for the use of the model to predict system's behavior under different climatological conditions.

The main limitation of our research comes from the selection of data captured in the test bed to validate the model; it was over a one-week period in January, when two common weather events did not occur: rain and ice sheets. These phenomena were not included in our model and both could potentially introduce a new set of problems.

The results obtained by simulation, and checked on a test bed, have also been compared to other similar systems research, and the degree of alignment found with those experiments has met expectations. Moreover, the introduced system can increase air flow temperature in an average of 4.8 °C with a peak value for the simulated period of 9.2 °C (having also the capability of increasing air temperature up to 19.9 °C. Considering that the data selected for the comparison was a worst case scenario (January, typically the coldest at the location of the experiment), the results are a reasonable cause for optimism regarding the practical applications of the solution. Finally, and in accordance with the results, the proposed model might be suitable to warm infantry UAV's hangar that motivated this design. To check this out, two lines of future works were initiated: first, in-depth research on shelter thermal properties, in order to validate transient simulations using them as envelopes; second, an investigation on the performance of the described system in different locations around the globe where this kind of military facilities could be deployed, in order to assess the suitability of the PV-T as a solution in these environments.

**Author Contributions:** Conceptualization, C.U., P.O.-C., J.M.N. and J.A.P.; methodology, C.U., P.O.-C., J.M.N. and J.A.P.; software, C.U. and P.O.-C.; validation, C.U., P.O.-C. and J.M.N.; formal analysis P.O.-C.; investigation, C.U. and P.O.-C.; resources, P.O.-C.; data curation, C.U. and P.O.-C.; writing—original draft preparation, C.U., P.O.-C.; writing—review and editing, C.U., P.O.-C., J.M.N. and J.A.P.; visualization, C.U. and P.O.-C.; supervision, J.M.N. and J.A.P. All authors have read and agree to the published version of the manuscript.

**Funding:** This research received no external funding.

**Conflicts of Interest:** The authors declare no conflict of interest.

#### Nomenclature

$\alpha$	solar absorptivity [-]
$\epsilon$	panel emissivity [-]
$\sigma$	Stefan-Boltzmann's constant [ $\text{W}/\text{m}^2\cdot\text{K}^4$ ]
$A_{PV}$	panel area [ $\text{m}^2$ ]
$c_p$	air flow specific heat [ $\text{J}/\text{kg}\cdot\text{K}$ ]
$h$	convection heat transfer [ $\frac{\text{W}}{\text{m}^2\cdot\text{K}}$ ]
$G$	irradiation [ $\text{W}/\text{m}^2$ ] $\dot{m}$ = mass air flow in cooling duct [ $\text{kg}/\text{s}$ ]
$T_{\text{amb}}$	ambient temperature [K]
$T_l$	lump mass temperature [K]
$T_{\text{ma}}$	average temperature of air fluid [K]
$T_{\text{out}}$	system's output temperature [°C]
$T_s$	temperature of surface in touch with air fluid [K]
$T_{\text{sky}}$	temperature in the surroundings of the system [K]
$V_w$	wind speed [ $\text{m}/\text{s}$ ] $\dot{q}_{\text{conv}}$ = system's convection losses [ $\text{W}/\text{m}^2$ ]
$\dot{Q}$	heat speed transfer [W]



## References

1. Chow, T.T. A review on photovoltaic/thermal hybrid solar technology. *Appl. Energy* **2010**, *87*, 365–379. [\[CrossRef\]](#)
2. Hasan, M.A.; Sumathy, K. Photovoltaic thermal module concepts and their performance analysis: A review. *Renew. Sustain. Energy Rev.* **2010**, *14*, 1845–1859. [\[CrossRef\]](#)
3. Kumar, R.; Rosen, M.A. A critical review of photovoltaic thermal solar collectors for air heating. *Appl. Energy* **2011**, *88*, 3603–3614. [\[CrossRef\]](#)
4. Parida, B.; Iniyar, S.; Goic, R. A review of solar photovoltaic technologies. *Renew. Sustain. Energy Rev.* **2011**, *15*, 1625–1636. [\[CrossRef\]](#)
5. Daghighi, R.; Ruslan, M.H.; Sopian, K. Advances in liquid based photovoltaic/thermal (PV/T) collectors. *Renew. Sustain. Energy Rev.* **2011**, *15*, 4156–4170. [\[CrossRef\]](#)
6. Ibrahim, A.; Othman, M.Y.; Ruslan, M.H.; Mat, S.; Sopian, K. Recent advances in flat plate photovoltaic/thermal (PV/T) solar collectors. *Renew. Sustain. Energy Rev.* **2011**, *15*, 352–365. [\[CrossRef\]](#)
7. Tyagi, V.V.; Kaushik, S.C.; Tyagi, S.K. Advancement in solar photovoltaic/thermal (PV/T) hybrid collector technology. *Renew. Sustain. Energy Rev.* **2012**, *16*, 1383–1398. [\[CrossRef\]](#)
8. Kamthania, D.; Tiwari, G.N. Photovoltaic thermal air collectors: A review. *J. Renew. Sustain. Energy* **2014**, *6*, 062701. [\[CrossRef\]](#)
9. Hamid, S.A.; Othman, M.Y.; Sopian, K.; Zaidi, S.H. An overview of photovoltaic thermal combination (PV/T combi) technology. *Renew. Sustain. Energy Rev.* **2014**, *38*, 212–222. [\[CrossRef\]](#)
10. Michael, J.J.; Iniyar, S.; Goic, R. Flat plate solar photovoltaic-thermal (PV/T) systems: A reference guide. *Renew. Sustain. Energy Rev.* **2015**, *51*, 62–88. [\[CrossRef\]](#)
11. Bhargava, A.K.; Garg, H.P.; Agarwal, R.K. Study of a hybrid solar system solar air heater combined with solar cells. *Energy Convers. Manag.* **1991**, *31*, 471–479. [\[CrossRef\]](#)
12. Sopian, K.; Yigit, K.S.; Liu, H.T.; Kakac, S.; Veziroglu, T.N. Performance analysis of photovoltaic thermal air heaters. *Energy Convers. Manag.* **1996**, *37*, 1657–1670. [\[CrossRef\]](#)
13. Othman, M.Y.H.; Yatim, B.; Sopian, K.; Bakar, M.N.A. Performance analysis of a double-pass photovoltaic/thermal (PV/T) solar collector with CPC and fins. *Renew. Energy* **2005**, *30*, 2005–2017. [\[CrossRef\]](#)
14. Tiwari, A.; Sodha, M.S. Parametric study of various configurations of hybrid PV/thermal air collector: Experimental validation of theoretical model. *Sol. Energy Mater. Sol. Cell* **2007**, *91*, 17–28. [\[CrossRef\]](#)
15. Tonui, J.K.; Tripanagnostopoulos, Y. Air-cooled PV/T solar collectors with low cost performance improvements. *Sol. Energy* **2007**, *81*, 498–511. [\[CrossRef\]](#)
16. Tonui, J.K.; Tripanagnostopoulos, Y. Performance improvement of PV/T solar collectors with natural air flow operation. *Sol. Energy* **2008**, *82*, 1–12. [\[CrossRef\]](#)
17. Katekar, V.P.; Deshmukh, S.S. A review on research trends in solar still designs for domestic and industrial applications. *J. Clean. Prod.* **2020**, 120544. [\[CrossRef\]](#)
18. Pang, W.; Cui, Y.; Zhang, Q.; Wilson, G.J.; Yan, H. A comparative analysis on performances of flat plate photovoltaic/thermal collectors in view of operating media, structural designs, and climate conditions. *Renew. Sustain. Energy Rev.* **2020**, *119*, 109599. [\[CrossRef\]](#)
19. Jia, Y.; Alva, G.; Fang, G. Development and applications of photovoltaic-thermal systems: A review. *Renew. Sustain. Energy Rev.* **2019**, *102*, 249–265. [\[CrossRef\]](#)
20. Yazdanifard, F.; Ameri, M. Exergetic advancement of photovoltaic/thermal systems (PV/T): A review. *Renew. Sustain. Energy Rev.* **2018**, *97*, 529–553. [\[CrossRef\]](#)
21. Sultan, S.M.; Efsan, M.E. Review on recent Photovoltaic/Thermal (PV/T) technology advances and applications. *Sol. Energy* **2018**, *173*, 939–954. [\[CrossRef\]](#)
22. Chauhan, A.; Tyagi, V.V.; Anand, S. Futuristic approach for thermal management in solar PV/thermal systems with possible applications. *Energy Convers. Manag.* **2018**, *163*, 314–354. [\[CrossRef\]](#)
23. Solanki, S.C.; Dubey, S.; Tiwari, A. Indoor simulation and testing of photovoltaic thermal (PV/T) air collectors. *Appl. Energy* **2009**, *86*, 2421–2428. [\[CrossRef\]](#)
24. Joshi, A.S.; Tiwari, A.; Tiwari, G.N.; Dincer, I.; Reddy, B.V. Performance evaluation of a hybrid photovoltaic thermal (PV/T) (glass-to-glass) system. *Int. J. Therm. Sci.* **2009**, *48*, 154–164. [\[CrossRef\]](#)
25. Sarhaddi, F.; Farahat, S.; Ajam, H.; Behzadmehr, A.M.I.N.; Adeli, M.M. An improved thermal and electrical model for a solar photovoltaic thermal (PV/T) air collector. *Appl. Energy* **2010**, *87*, 2328–2339. [\[CrossRef\]](#)

26. Shahsavari, A.; Ameri, M. Experimental investigation and modeling of a direct coupled PV/T air collector. *Sol. Energy* **2010**, *84*, 1938–1958. [CrossRef]
27. Kumar, R.; Rosen, M.A. Performance evaluation of a double pass PV/T solar air heater with and without fins. *Appl. Therm. Eng.* **2011**, *31*, 1402–1410. [CrossRef]
28. Kamthania, D.; Nayak, S.; Tiwari, G.N. Performance evaluation of a hybrid photovoltaic thermal double pass facade for space heating. *Energy Build.* **2011**, *43*, 2274–2281. [CrossRef]
29. Daghighi, R.; Khaledian, Y. Design and fabrication of a bi-fluid type photovoltaic-thermal collector. *Energy* **2017**, *135*, 112–127. [CrossRef]
30. Kuo, C.F.J.; Liu, J.M.; Umar, M.L.; Lan, W.L.; Huang, C.Y.; Syu, S.S. The photovoltaic-thermal system parameter optimization design and practical verification. *Energy Convers. Manag.* **2019**, *180*, 358–371. [CrossRef]
31. Thiers, S.; Aoun, B.; Peuportier, B. Experimental characterization, modeling and simulation of a wood pellet micro-combined heat and power unit used as a heat source for a residential building. *Energy Build.* **2010**, *42*, 896–903. [CrossRef]
32. Lombardi, K.; Ugursal, V.I.; Beausoleil-Morrison, I. Proposed improvements to a model for characterizing the electrical and thermal energy performance of Stirling engine micro-cogeneration devices based upon experimental observations. *Appl. Energy* **2010**, *87*, 3271–3282. [CrossRef]
33. Magri, G.; di Perna, C.; Serenelli, G. Analysis of electric and thermal seasonal performances of a residential microchip unit. *Appl. Therm. Eng.* **2012**, *36*, 193–201. [CrossRef]
34. Ulloa, C.; Porteiro, J.; Eguía, P.; Pousada-Carballo, J.M. Application model for a stirling engine micro-generation system in caravans in different european locations. *Energies* **2013**, *6*, 717–732. [CrossRef]
35. Ulloa, C.; Míguez, J.L.; Porteiro, J.; Eguía, P.; Cacabelos, A. Development of a Transient Model of a Stirling-Based CHP System. *Energies* **2013**, *6*, 3115–3133. [CrossRef]
36. Keynejad, F.; Manzie, C. Cold start modeling of spark ignition engines. *Control Eng. Pract.* **2011**, *19*, 912–925. [CrossRef]
37. Hasan, A.; Vuolle, M.; Sirén, K. Minimisation of life cost of a detached house using combined simulation and optimization. *Build. Environ.* **2008**, *43*, 2022–2034. [CrossRef]
38. Yan, F.; Wang, J. Pressure-based transient intake manifold temperature reconstruction in Diesel engines. *Control Eng. Pract.* **2012**, *20*, 531–538. [CrossRef]
39. Wang, X.; Chua, H.T. Two bed silica gel-water adsorption chillers: An effectual lumped parameter model. *Int. J. Refrig.* **2007**, *30*, 1417–1426. [CrossRef]
40. HDT. HDT Global. 2017. Available online: <https://www.hdtglobal.com/> (accessed on 1 February 2019).
41. Ulloa, C.; Nuñez, J.M.; Lin, C.; Rey, G. AHP-based design method of a lightweight, portable and flexible air-based PV-T module for UAV shelter hangars. *Renew. Energy* **2018**, *123*, 767–780. [CrossRef]
42. Petru, L.; Mazen, G. PWM control of a DC motor used to drive a conveyor belt. *Procedia Eng.* **2015**, *100*, 299–304. [CrossRef]
43. Salamone, F.; Belussi, L.; Danza, L.; Ghellere, M.; Meroni, I. An open source low cost wireless control system for a forced circulation solar plant. *Sensors* **2015**, *15*, 27990–28004. [CrossRef]
44. Avallone, E.; Cunha, D.G.; Padilha, A.; Scalón, V.L. Electronic multiplex system using the Arduino platform to control and record the data of the temperatures profiles in heat storage tank for solar collector. *Int. J. Energy Environ. Eng.* **2016**, *7*, 391–398. [CrossRef]
45. Claros-Marfil, L.J.; Padial, J.F.; Lauret, B. A new and inexpensive open source data acquisition and controller for solar research: Application to a water-flow glazing. *Renew. Energy* **2016**, *92*, 450–461. [CrossRef]
46. Swinbank, W. Long-wave radiation from clear skies. *Q. J. R. Meteorol. Soc.* **1963**, *89*, 339–348. [CrossRef]
47. Nusselt, W.; Jürges, W. Die Kühlung einer Ebenen Wand Durch einen Luftstrom (The Cooling of a Plane Wall by an Air Flow). In *Gesundheits Ingenieur*; 52. Heft, 45. Jahrgang; Umwelttechnik (München); DIV: München, Germany, 30 December 1922; pp. 641–642.

